CrossMark

ARTICLE

A Facile Synthesis of ZnCo$_2$O$_4$ Nanocluster Particles and the Performance as Anode Materials for Lithium Ion Batteries

Yue Pan[1,2] · Weijia Zeng[1] · Lin Li[1] · Yuzi Zhang[3] · Yingnan Dong[2] · Dianxue Cao[1] · Guiling Wang[1] · Brett L. Lucht[2] · Ke Ye[1] · Kui Cheng[1]

Highlights

- ZnCo$_2$O$_4$ nanocluster particles (NCPs) were prepared through a hydrothermal method with the assistance of sodium dodecyl benzene sulfonate (SDBS).
- The ZnCo$_2$O$_4$ NCPs exhibit excellent rate performance. The initial lithiation-specific capacity of ZnCo$_2$O$_4$ NCPs with a current density of 100 mA g^{-1} reached 1110 mAh g^{-1} with a coulombic efficiency of 84.7 %, and a high delithiation capacity of 700 mAh g^{-1} was achieved over 100 cycles.

Abstract ZnCo$_2$O$_4$ nanocluster particles (NCPs) were prepared through a designed hydrothermal method, with the assistance of a surfactant, sodium dodecyl benzene sulfonate. The crystalline structure and surface morphology of ZnCo$_2$O$_4$ were investigated by XRD, XPS, SEM, TEM, and BET analyses. The results of SEM and TEM suggest a clear nanocluster particle structure of cubic ZnCo$_2$O$_4$ ($\sim$100 nm in diameter), which consists of aggregated primary nanoparticles ($\sim$10 nm in diameter), is achieved. The electrochemical behavior of synthesized ZnCo$_2$O$_4$ NCPs was investigated by galvanostatic discharge/charge measurements and cyclic voltammetry. The ZnCo$_2$O$_4$ NCPs exhibit a high reversible capacity of 700 mAh g^{-1} over 100 cycles under a current density of 100 mA g^{-1} with an excellent coulombic efficiency of 98.9% and a considerable cycling stability. This work demonstrates a facile technique designed to synthesize ZnCo$_2$O$_4$ NCPs which show great potential as anode materials for lithium ion batteries.

Graphical Abstract
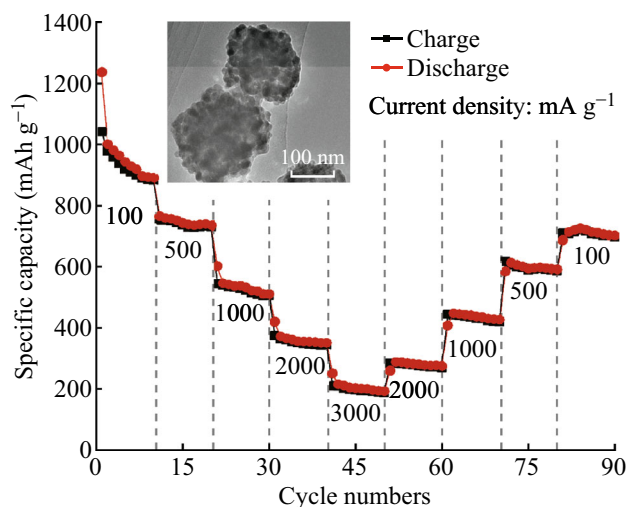
✉ Guiling Wang
wangguiling@hrbeu.edu.cn

✉ Brett L. Lucht
blucht@chm.uri.edu

1 Key Laboratory of Superlight Materials and Surface Technology of Ministry of Education, College of Materials Science and Chemical Engineering, Harbin Engineering University, Harbin 150001, People's Republic of China

2 Department of Chemistry, University of Rhode Island, Kingston, RI 02881, USA

3 Department of Chemical Engineering, University of Rhode Island, Kingston, RI 02881, USA

🙋 Springer

1 Introduction

It is well known that novel renewable energy sources and energy storage materials are two major challenges in electrochemical technology. Rechargeable lithium ion batteries (LIBs), which have been recognized as vitally important devices of power sources, have attracted widespread attention. LIBs with high energy and power density, low cost, and short charging time are needed urgently to meet the rapid development of hybrid and electric vehicles. In principle, the electrochemical performance of safe LIBs depends largely on the electrode materials for lithium storage.

Among the array of promising anode materials for LIBs, transition metal oxides have been widely studied due to their higher specific capacities compared to traditional graphite with a specific capacity of 372 mAh g^{-1}. Ternary oxides, AB_2O_4 (A=Mg, Mn, Fe, Co, Ni, Cu, or Zn; B=Mn, Fe, Co, Ni, or Cu; A≠B), with a variety of crystal structures (spinel, scheelite, brannerite, etc.) have been investigated as anode materials for LIBs [1–4]. This class of materials contains at least one transition metal ion and one or more electrochemically active/inactive ions. AB_2O_4 in previous electrochemical studies were synthesized via molten salt method [5–8], oxalate decomposition method [9, 10], combustion method [11, 12], solvothermal method [13], etc. And they were found to show good Li cyclability with relatively high specific capacities.

The typical ternary oxide, zinc cobaltite ($ZnCo_2O_4$), possesses a spinel structure, where the Zn^{2+} occupies the tetrahedral sites and the Co^{3+} occupies the octahedral sites. $ZnCo_2O_4$ has been demonstrated to be a promising candidate as anode materials for LIBs because of the outstanding electrochemical performance (the theoretical specific capacity of 975 mAh g^{-1}) and the abundant source, low cost, and low toxicity of zinc. Generally, the electrochemical performance of electrode materials depends on the preparation technique, the size and shape of particles and the morphology. The strategies deployed to prepare $ZnCo_2O_4$ are similar to those designed to synthesize AB_2O_4 mentioned above [1, 14].

Hao [15] reported porous $ZnCo_2O_4$ microspheres synthesized by a solvothermal method, with a high reversible capacity of 940 mAh g^{-1} at 0.1 °C. In Huang's work [16], core–shell $ZnCo_2O_4$ microspheres were fabricated by a hydrothermal method. They showed an initial discharge capacity of 1280 mAh g^{-1} at 200 mA g^{-1}, and only 3.9% capacity was lost between the 2nd and the 5th cycles at 400 mA g^{-1}. According to Zhao's study [17], highly ordered mesoporous spinel $ZnCo_2O_4$ was prepared with SBA-15 as templates. It displayed a high reversible capacity of 1623 mAh g^{-1} at 2.0 A g^{-1}. The capacity still remained at 1470 mAh g^{-1} with a high current density of 8.0 A g^{-1}. Wang's group [18] prepared hierarchical porous $ZnCo_2O_4$ microspheres by simply decomposing PBA followed by sintering at 550 °C, which showed an initial lithiation and delithiation capacity of 1737.1 and 1051.6 mAh g^{-1}, respectively, after 100 cycles at 100 mA g^{-1}. In general, nanosized $ZnCo_2O_4$ with uniquely designed structures showed promising results in enhancing the electrochemical performance due to the high surface-to-volume ratio and the excellent electronic transport property. However, the limitation for the industrial application of this anode material is the control in preparation of the active material.

Herein, a facile approach is designed to synthesize uniform $ZnCo_2O_4$ NCPs. The cycling stability study of our $ZnCo_2O_4$ NCPs shows a delithiation capacity of 700 mAh g^{-1} over 100 cycles under a current density of 100 mA g^{-1}. Excellent electrochemical performance of $ZnCo_2O_4$ NCPs demonstrates that it is promising to employ this material in high-energy storage devices.

2 Experiments

2.1 Preparation of $ZnCo_2O_4$ NCPs and Structure Characterization

With the assistance of sodium dodecyl benzene sulfonate (SDBS), a non-aqueous hydrothermal method was designed for the synthesis of $ZnCo_2O_4$ NCPs. In a typical synthesis procedure, $ZnCl_2 \cdot H_2O$, $CoCl_2 \cdot H_2O$, urea, and SDBS were added into ethylene glycol. Afterwards, the mixture was stirred until the complete dissolution of all reagents occurred. After being transferred into a Teflon-lined autoclave, the pink and purple solution was subsequently kept constant at 200 °C for 24 h. After completely cooling down, the resulting pink precipitates were washed several times with a mixture of deionized water and absolute ethanol, and dried in a vacuum oven at 90 °C overnight. $ZnCo_2O_4$ NCPs were obtained by annealing the pink precipitates at 500 °C for 2 h in air. The hypothesized evolution of $ZnCo_2O_4$ NCPs is further illustrated in Scheme 1.

The morphology and structure of $ZnCo_2O_4$ NCPs were examined by a combination of scanning electron microscopy (SEM), transmission electron microscopy (TEM), and X-ray diffraction (XRD). Thermal analysis of the pink precursor power was characterized by thermogravimetry–differential thermal analysis (TG–DTA). The specific surface area of pure $ZnCo_2O_4$ NCPs powder was measured on Micromeritics Instrument Corporation TriStar II 3020 using N_2 adsorption–desorption isotherms at −196 °C.

2.2 Electrochemical Characterization

CR2032 coin cell was used to carry out the electrochemical experiments with Li foil serving as a reference and a counter electrode. Slurries of the active material ($ZnCo_2O_4$ NCPs), carbon black, and poly (vinyl difluoride) (PVDF; weight ratio of 70:20:10) in N-methyl-2-pyrrolidone were pasted on pure Cu foil with a thickness of 150 μm and dried under vacuum at 95 °C overnight to make working electrodes. The active material loading was 1.0–1.5 mg cm^{-2}. 1.0 mol L^{-1} LiPF$_6$ dissolved in a mixture of ethylene carbonate (EC), dimethyl carbonate (DMC), and ethyl methyl carbonate (EMC; volume ratio of 1:1:1) was used as the electrolyte. The cells were assembled in an Ar-filled glove box, with one microporous polypropene film (Celgard 2400) and one glass fiber as separator. An electrochemical workstation (VMP3/Z, Bio-logic, France) and a battery test system (CT-3008-5 V/5 mA, Neware Technology Ltd., Shenzhen, China) were used to test the electrochemical performance of all the cells under different current densities from 0.005 to 3.0 V vs. Li$^+$/Li.

3 Results and Discussion

3.1 Structure and Morphology of ZnCo$_2$O$_4$

To determine a suitable calcination temperature to prepare $ZnCo_2O_4$ powder, TG–DTA was used and the result is shown in Fig. 1a. A small peak occurs at 367 °C, and two main exothermal peaks are at ~ 324 and ~ 402 °C, respectively. They are corresponding to the conversion of intermediates (metal glycoalates or alkoxides derivatives from the reaction of ethylene glycol with the metal ions) into $ZnCo_2O_4$ [19, 20]. Meanwhile, these peaks were accompanied by a drastic mass lose of about 29% in the temperature range 300–405 °C. In order to ensure that the precursor can be completely decomposed, the calcination temperature was finally set at 500 °C to prepare $ZnCo_2O_4$ NCPs.

Figure 1b shows the XRD pattern of synthesized $ZnCo_2O_4$ NCPs. The exhibited diffraction peaks can be indexed as a single cubic phase of $ZnCo_2O_4$ with the lattice constant a = 8.06 Å, in good agreement with the standard value of 8.09 Å (JCPDS card No. 23-1390). No peaks from
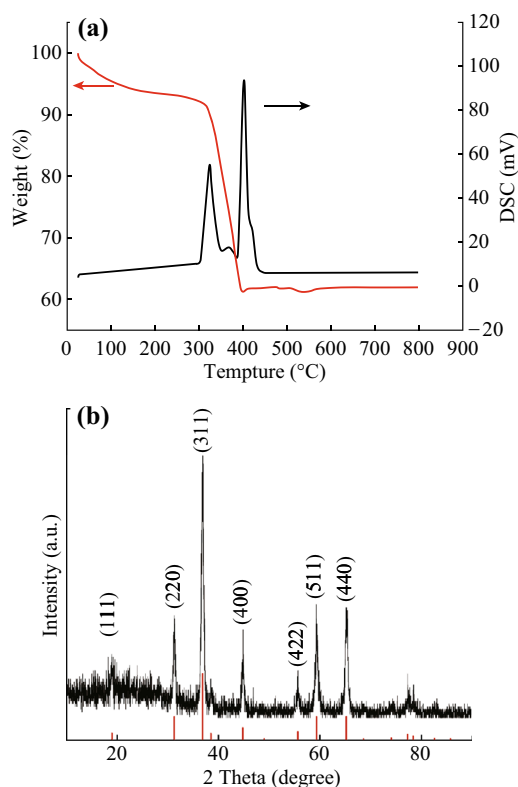

Fig. 1 a TG–DTA of the precursor; b XRD of $ZnCo_2O_4$ NCPs

other phases are detected, implying the high purity of synthesized $ZnCo_2O_4$ NCPs. Based on the Scherrer formula, the average diameter of $ZnCo_2O_4$ NCPs is around 13 nm calculated from the XRD pattern.

To investigate the composition and surface electronic state of $ZnCo_2O_4$ NCPs, XPS analysis was conducted. In the O 1s spectrum (Fig. 2), there are two main peaks at 529.2 and 530.8 eV, which should be attributed to the lattice oxygen from $ZnCo_2O_4$ NCPs and the oxygen from hydroxide ions, respectively. The two minor O 1s peaks around 532.2 and 533.7 eV are believed to be generated from surface bound water or adsorbed oxygen [21–23]. There are two major peaks at binding energies of 1044.4 and 1021.3 eV in the Zn 2p spectrum, attributed to Zn 2p1/2 and Zn 2p3/2 of Zn^{2+} [24]. The binding energy values of the two major peaks are 780.4 and 795.2 eV in the Co 2p spectrum, associated with Co 2p3/2 and Co 2p1/2, respectively. Additionally, the spineorbit splitting of the
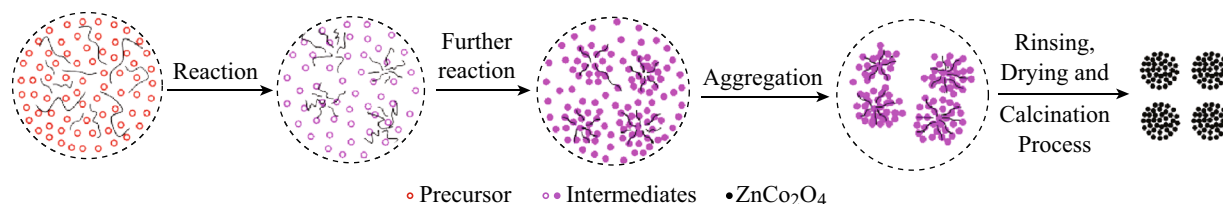
Scheme 1 Illustration of the formation process of $ZnCo_2O_4$ NCPs

mentioned two peaks is 14.8 eV. Two accompanied weak satellite peaks are also visible at 790.0 and 805.0 eV and the energy gap between the main peak and the satellite peaks is around 9.8 eV. This suggests that Co cation can be assigned a value of +3 [15]. The results are quite close to those reported about MCo_2O_4 (M=Mg, Cu, Zn) [8]. In addition, the survey spectrum shows the presence of Zn, Co, and O as well as C.

The morphology of $ZnCo_2O_4$ NCPs was characterized by SEM and TEM, as shown in Fig. 3. The SEM images of the precursor and $ZnCo_2O_4$ are exhibited, respectively, in Fig. 3a, b. A uniform powder has been synthesized by the hydrothermal method with the assistance of SDBS. The sizes of precursor and $ZnCo_2O_4$ particles are approximately the same, and the fluffy surface turns to be tighter with the process of calcinations. From Fig. 3c, the $ZnCo_2O_4$ NCPs comprise small primary nanoparticles with a diameter around 10 nm. Figure 3d shows a typical HRTEM image of the $ZnCo_2O_4$ particles, revealing a structurally uniform lattice spacing of about 0.47 nm, which corresponds to the (111) lattice plane of the $ZnCo_2O_4$. Meanwhile, the crystallization of $ZnCo_2O_4$ is also well confirmed. The BET surface area of $ZnCo_2O_4$ NCPs is 30.0 m^2 g^{-1}, which is similar to those of other metal oxides or oxysalts as electrode materials for LIBs reported recently [25–31].

3.2 Electrochemical Performance of $ZnCo_2O_4$ NCPs

The electrochemical performance of the $ZnCo_2O_4$ NCPs as the anode materials for LIBs was evaluated by galvanostatic discharge/charge experiments. The curves were measured at room temperature with a current density of 100 mA g^{-1} ranging from 0.005 to 3 V(vs. Li^+/Li). Figure 4 shows the voltage-capacity profile of prepared $ZnCo_2O_4$ NCPs electrode for the first three lithiation/ delithiation cycles. There is a stable potential plateau around 0.85 V during the first discharge process and the long discharging plateau becomes steeper and moves upward, consequently forming a long slope between 1.25 and 0.60 V in the following two cycles. The first lithiation capacity reaches as high as 1110($\pm$5) mAh g^{-1} with a coulombic efficiency of 84.7% in the 1st cycle. The irreversible capacity may be attributed to the kinetic limitations of reactions [32], the formation of solid electrolyte interphase (SEI), the polymeric layer formation on the metal and nanoparticles (active material) under the deep discharge conditions (0.005 V vs. Li) [33], and the reduction of active metal to metal with Li_2O formation, which is commonly observed for several types of electrode materials [34–36]. The lithiation and delithiation capacities in the 2nd cycle are 932 and 912($\pm$5) mAh g^{-1}, respectively.
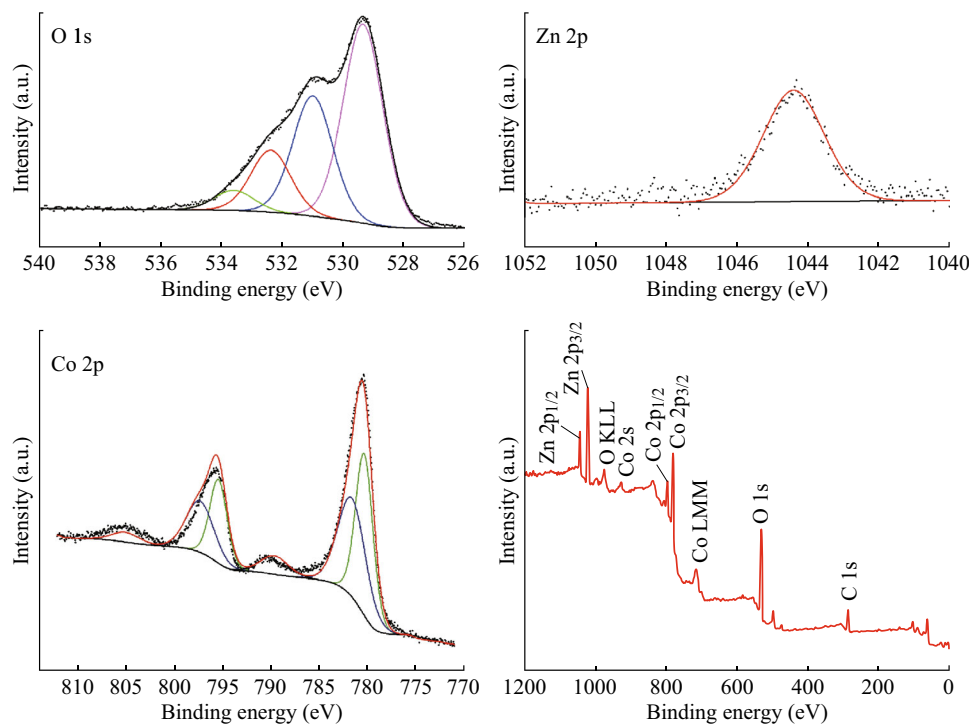

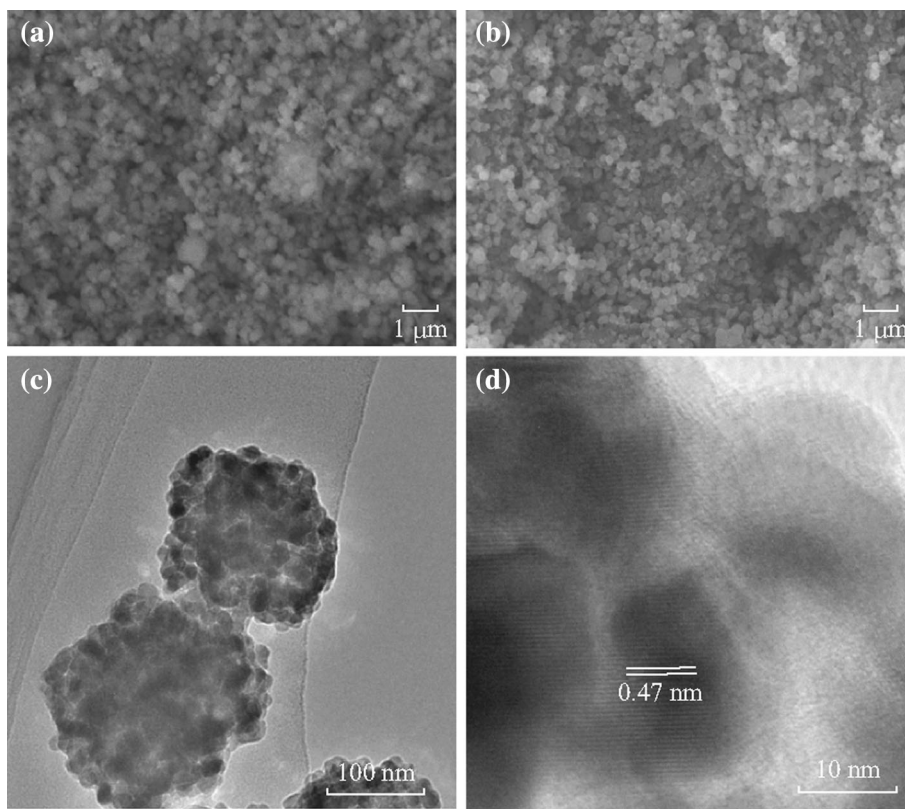Fig. 2 XPS spectra: O 1s, Zn 2p, Co 2p, and survey spectrum for the as-synthesized $ZnCo_2O_4$ NCPs

Fig. 3 **a** SEM of the precursor. **b** SEM of ZnCo$_2$O$_4$ NCPs. **c** TEM of ZnCo$_2$O$_4$ NCPs. **d** HRTEM of ZnCo$_2$O$_4$ NCPs
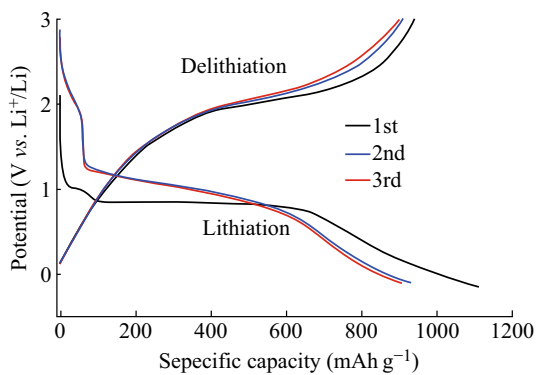
Fig. 4 The first three lithiation/delithiation curves of ZnCo$_2$O$_4$ NCPs

Fig. 5 Cycling performance at 0.1 °C for ZnCo$_2$O$_4$ NCPs

And the values change to 908 and 901($\pm$5) mAh g^{-1}, with a higher coulombic efficiency of 99.3% in the 3rd cycle. The capacities are continuously lost through the pulverization and aggregation of ZnCo$_2$O$_4$ NCPs, as well as the reduced electrical contact.

The cycling stability and corresponding coulombic efficiency of ZnCo$_2$O$_4$ NCPs are demonstrated in Fig. 5. The ZnCo$_2$O$_4$ electrode reveals a large capacity fading during the initial 16 cycles. For the 16th cycle, the retention of delithiation capacity is 85.2%. In the following cycles, the reversible capacities decrease at a slower rate and a retention value about 81.0% is maintained in the 50th
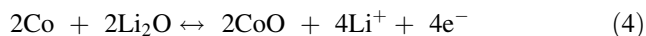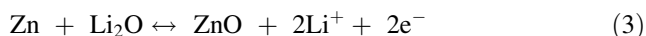
cycle. The decay rate of delithiation capacities increases until the 76th cycle, where it has a slight rebound with the continuous cycling. After 100 cycles, a high delithiation capacity of 700($\pm$5) mAh g^{-1} is still retained with a retention of 74.4%, demonstrating the high specific capacity and superior cyclability of ZnCo$_2$O$_4$ NCPs. The coulombic efficiencies are ranging from 99.3% to 98.4% except in the first two cycles. The outstanding electrochemical behavior of ZnCo$_2$O$_4$ NCPs could be attributed to the unique structure (shown in Fig. 2c), which has possessed high specific surface area and empty space among

the aggregated nanosized primary $ZnCo_2O_4$ particles. In this way, $ZnCo_2O_4$ NCPs can provide a short pathway for Li^+ diffusion and a large electrode–electrolyte contact area for Li^+ migration across the interface. More importantly, the empty space between adjacent particles can significantly improve the structural integrity caused by the volume change associated with the repeated lithiation and delithiation processes.

The rate performance of $ZnCo_2O_4$ NCP electrode is provided in Fig. 6. The reversible delithiation capacity is $884(\pm 5)$ mAh g^{-1} at the 10th cycle under 100 mA g^{-1}, and this value decreases to 731, 506, 345, $188(\pm 5)$ mAh g^{-1} with a continuously increasing current density from 500 to 3000 mA g^{-1}. More importantly, as the current density gradually decreases from 3000 back to 100 mA g^{-1}, the $ZnCo_2O_4$ NCP electrode also shows good performance with slight decay. A reversible delithiation capacity of $698(\pm 5)$ mAh g^{-1} could be resumed and maintained at the last cycle when the current is back to 100 mA g^{-1}. This result demonstrates the excellent performance of $ZnCo_2O_4$ NCPs.

According to previous studies [14, 15, 37], the electrochemical reactions of $ZnCo_2O_4$ involved in the lithium insertion and extraction reactions can be illustrated as follows:

$$ZnCo_2O_4 + 8Li^+ + 8e^- \rightarrow Li_xZnCo_2O_4$$
$$\rightarrow Zn + 2Co + 4Li_2O \quad (1)$$

$$Zn + Li^+ + e^- \leftrightarrow LiZn \quad (2)$$

$$Zn + Li_2O \leftrightarrow ZnO + 2Li^+ + 2e^- \quad (3)$$

$$2Co + 2Li_2O \leftrightarrow 2CoO + 4Li^+ + 4e^- \quad (4)$$

$$2CoO + 2/3Li_2O \leftrightarrow 2/3Co_3O_4 + 4/3Li^+ + 4/3e^- \quad (5)$$
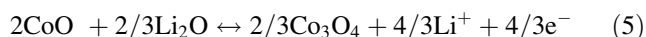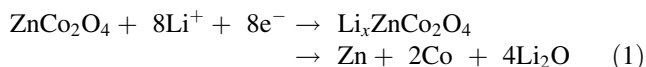
Cyclic voltammetry can provide additional detail on the electrochemical reactions of $ZnCo_2O_4$ NCPs with the

Fig. 7 Cyclic Voltammograms of $ZnCo_2O_4$ NCPs electrode at a scan rate of 0.1 mV s^{-1}

electrolyte. Figure 7 presents the first three cyclic voltammograms of $ZnCo_2O_4$ NCPs electrode in the voltage of 0.005–3.0 V at a scan rate of 0.1 mV s^{-1}. The initial cathodic process observed on the electrode starts at ~ 0.8 V and a sharp peak occurs at ~ 0.6 V versus Li, which should be resulted from the intercalation reaction of $Li_xZnCo_2O_4$, the reduction of Zn^{2+} and Co^{3+} to Zn^0 and Co^0 (Eq. 1), the formation of Li–Zn alloys (Eq. 2), and an irreversible reaction related to the decomposition of the electrolyte [14, 38]. In the anodic sweep, two main oxidation peaks are observed at 1.7 and 2.0 V characteristic of the oxidation process of Zn and Co to Zn^{2+} and Co^{3+} (Eqs. 3–5) [39]. The second CV scan contains a cathodic peak ~ 1.0 V, distinguishing the reduction mechanism from that in the 1st cycle [40] and two anodic peaks at 1.7 and 2.0 V. Similar CV scan is observed in the 3rd cycle
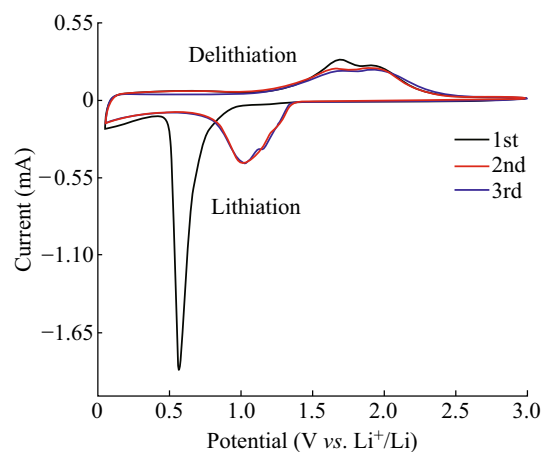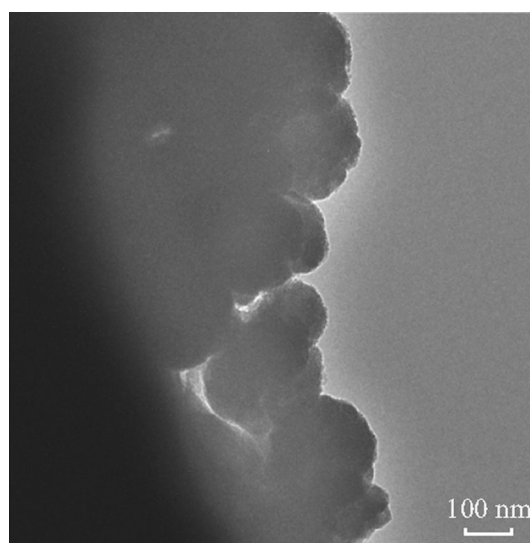

Fig. 6 Rate performance of $ZnCo_2O_4$ NCPs electrode at various current densities

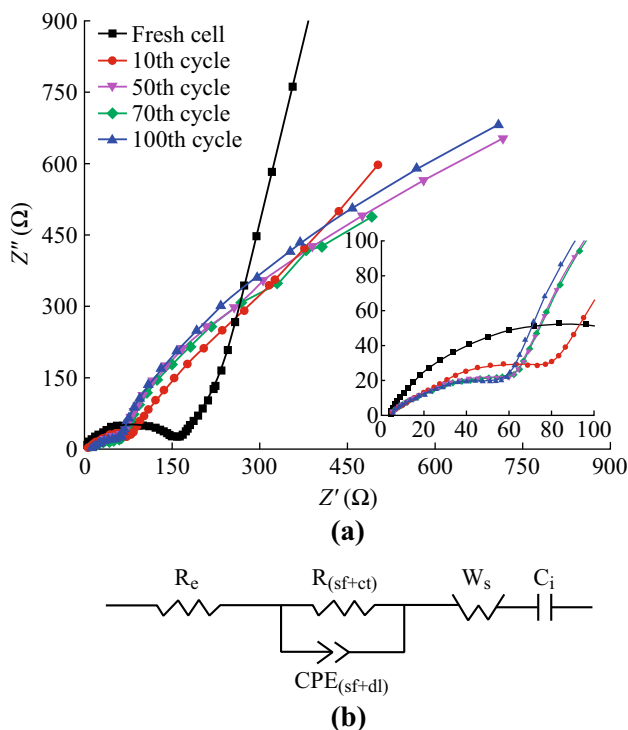**Fig. 8** TEM image of $ZnCo_2O_4$ NCPs electrode after 100 cycles at 100 mA g^{-1}

Fig. 9 **a** Electrochemical impedance spectra of $ZnCo_2O_4$ NCPs electrode after different cycles. **b** Equivalent electrical circuit used to fit the data of Fig. 9a

although the intensity of all peaks decreases slightly, typical for reversible lithium ion intercalation/deintercalation and reversible cycling of the cells above.

In order to investigate the morphology changes after continuous discharge and charge cycles, the cell of $ZnCo_2O_4$ NCPs after 100 cycles at 100 mA g^{-1} was disassembled and monitored by TEM. As revealed in Fig. 8, $ZnCo_2O_4$ NCPs anode after 100 cycles still shows well spherical morphology with a diameter $\sim$ 100 nm. However, the primary clustered structure is not obvious after cycling test, which can be attributed to the irreversible structure destruction during the cycling process. In sum,

these results strongly explain the reasons for the excellent electrochemical properties of $ZnCo_2O_4$ NCPs.

Nyquist plots of $ZnCo_2O_4$ NCPs electrode at open-circuit voltage (OCV, 2.8–3.0 V) after different cycles at 0.1 °C are shown in Fig. 9a, to investigate how the impedance changes with continuous cycling. The impedance spectra were fitted to an equivalent circuit, consisting of the resistances for electrolyte, cell components, surface film (sf), and charge-transfer(ct); a constant phase element (CPE$_i$); Warburg impedance (W_s) and intercalation capacitance (C_i) [32, 33]. The circuit is shown in Fig. 9b. The fitted impedance data values are listed in Table 1. The R_b values were relatively stable ($\sim$4.0 Ω) and $R_{(sf+ct)}$ values were found to decrease with continuous cycle. The decrease of R_{ct} may be related to the wetting process between the $ZnCo_2O_4$ NCPs (active material) and electrolyte, as well as the lower polarization and higher reactivity of $ZnCo_2O_4$ NCPs. The CPE$_{(sf+ct)}$ values increased from 12 μF (fresh cell) to 160 μF (after 10 cycles), corresponding to the formation of SEI film. After the 50th cycle, the values are almost stable. As cycling, the electrolyte can soak into the $ZnCo_2O_4$ particles, and the active $ZnCo_2O_4$ is converted to lower oxidation state, cobalt oxide, zinc oxide, and Li_2O. This result is consistent with the cycling performance (Fig. 4).

4 Conclusions

In summary, $ZnCo_2O_4$ NCPs are synthesized successfully by a designed hydrothermal method with the assistance of SDBS. The characterizations by XRD, SEM, and TEM show uniform $ZnCo_2O_4$ NCPs around 100 nm in diameter, comprising aggregated primary $ZnCo_2O_4$ nanoparticles ($\sim$ 10 nm in diameter). The electrochemical measurements reveal that the first lithiation and delithiation capacities of $ZnCo_2O_4$ NCPs are 1110 and 941 mAh g^{-1}, respectively. After 100 cycles, a high reversible delithiation capacity of 700 mAh g^{-1} is retained. The high capacities and good

Table 1 Impedance parameters of $ZnCo_2O_4$–Li after different cycles in the fully charged state

	Fresh cell	10th-charge cycle	50th-charge cycle	70th-charge cycle	100th-charge cycle
OCV (V vs. Li) open-circuit voltage	2.2	2.85	2.90	2.80	2.90
R_e (Ω) electrolyte resistance	3.9	4.4	4.0	4.2	4.1
$R_{(sf+ct)}$ (Ω) surface film + charge transfer resistance	149.4	72.8	47.1	47.9	48.2
CPE$_{(sf+dl)}$ (μF) constant phase element due to surface film + double layer capacitance	12	160	125	113	102
W_s (Ω) Warburg resistance	690	2969	3826	3838	3894
C_i (μF) intercalation capacitance	284	4.7	3.5	3.0	2.8

stability are attributed to the unique nanostructures of $ZnCo_2O_4$, which demonstrate the promising application of our synthesized $ZnCo_2O_4$ as anode materials for LIBs.

References

1. M.V. Reddy, G.V. Subba Rao, B.V. Chowdari, Metal oxides and oxysalts as anode materials for Li ion batteries. Chem. Rev. **113**(7), 5364–5457 (2013). doi:10.1021/cr3001884

2. D. Zhao, Y. Wang, Y. Zhang, High-performance Li-ion batteries and supercapacitors base on 1-D nanomaterials in prospect. Nano-Micro Lett. **3**(1), 62–71 (2011). doi:10.3786/nml.v3i1.p62-71

3. Y. Pan, Y. Zhang, X. Wei, C. Yuan, J. Yin, D. Cao, G. Wang, $MgFe_2O_4$ nanoparticles as anode materials for lithium-ion batteries. Electrochim. Acta **109**, 89–94 (2013). doi:10.1016/j.electacta.2013.07.026

4. Y. Xiao, X. Li, J. Zai, K. Wang, Y. Gong, B. Li, Q. Han, X. Qian, $CoFe_2O_4$-graphene nanocomposites synthesized through an ultrasonic method with enhanced performances as anode materials for Li-ion batteries. Nano-Micro Lett. **6**(4), 307–315 (2014). doi:10.1007/s40820-014-0003-7

5. M.V. Reddy, C. Yu, F. Jiahuan, K.P. Loh, B.V.R. Chowdari, Molten salt synthesis and energy storage studies on CuCo2O4 and CuO·Co3O4. RSC Adv. **2**(25), 9619–9625 (2012). doi:10.1039/c2ra21033a

6. M.V. Reddy, C.Y. Quan, K.W. Teo, L.J. Ho, B.V.R. Chowdari, Mixed oxides, $(Ni_{1-x}Zn_x)Fe_2O_4$ ($x = 0$, 0.25, 0.5, 0.75, 1): molten salt synthesis, characterization and its lithium-storage performance for lithium ion batteries. J. Phys. Chem. C **119**(9), 4709–4718 (2015). doi:10.1021/jp5121178

7. M.V. Reddy, M. Rajesh, S. Adams, B.V.R. Chowdari, Effect of initial reactants and reaction temperature on molten salt synthesis of $CuCo_2O_4$ and its sustainable energy storage properties. ACS Sustain. Chem. Eng. **4**(6), 3076–3086 (2016). doi:10.1021/acssuschemeng.6b00047

8. M.V. Reddy, Y. Xu, V. Rajarajan, T. Ouyang, B.V.R. Chowdari, Template free facile molten synthesis and energy storage studies on MCo_2O_4 (M=Mg, Mn) as anode for li-ion batteries. ACS Sustain. Chem. Eng. **3**(12), 3035–3042 (2015). doi:10.1021/acssuschemeng.5b00439

9. D. Darbar, M.V. Reddy, S. Sundarrajan, R. Pattabiraman, S. Ramakrishna, B.V.R. Chowdari, Anodic electrochemical performances of $MgCo_2O_4$ synthesized by oxalate decomposition method and electrospinning technique for Li-ion battery application. Mater. Res. Bull. **73**, 369–376 (2016). doi:10.1016/j.materresbull.2015.09.025

10. P. Peshev, A. Toshev, G. Gyurov, Preparation of high-dispersity MCo_2O_4 (M=Mg, Ni, Zn) spinels by thermal dissociation of coprecipitated oxalates. Mater. Res. Bull. **24**(1), 33–40 (1989). doi:10.1016/0025-5408(89)90005-6

11. C.T. Cherian, M.V. Reddy, G.V.S. Rao, C.H. Sow, B.V.R. Chowdari, Li-cycling properties of nano-crystalline $(Ni_{1-x}Zn_x)$-Fe_2O_4 ($0 \leq x \leq 1$). J. Solid State Electrochem. **16**(5), 1823–1832 (2012). doi:10.1007/s10008-012-1662-2

12. Y. Sharma, N. Sharma, G.V.S. Rao, B.V.R. Chowdari, Lithium recycling behaviour of nano-phase-$CuCo_2O_4$ as anode for lithium-ion batteries. J. Power Sources **173**(1), 495–501 (2007). doi:10.1016/j.jpowsour.2007.06.022

13. H. Zhao, L. Liu, X. Xiao, Z. Hu, S. Han, Y. Liu, D. Chen, X. Liu, The effects of Co doping on the crystal structure and electrochemical performance of $Mg(Mn_{2-x}Co_x)O_4$ negative materials for lithium ion battery. Solid State Sci. **39**, 23–28 (2015). doi:10.1016/j.solidstatesciences.2014.11.006

14. M.V. Reddy, K.Y.H. Kenrick, T.Y. Wei, G.Y. Chong, G.H. Leong, B.V.R. Chowdari, Nano-$ZnCo_2O_4$ material preparation by molten salt method and its electrochemical properties for lithium batteries. J. Electrochem. Soc. **158**(12), A1423 (2011). doi:10.1149/2.089112jes

15. S. Hao, B. Zhang, S. Ball, M. Copley, Z. Xu, M. Srinivasan, K. Zhou, S. Mhaisalkar, Y. Huang, Synthesis of multimodal porous $ZnCo_2O_4$ and its electrochemical properties as an anode material for lithium ion batteries. J. Power Sources **294**, 112–119 (2015). doi:10.1016/j.jpowsour.2015.06.048

16. L. Huang, G.H. Waller, Y. Ding, D. Chen, D. Ding, P. Xi, Z.L. Wang, M. Liu, Controllable interior structure of $ZnCo_2O_4$ microspheres for high-performance lithium-ion batteries. Nano Energy **11**, 64–70 (2015). doi:10.1016/j.nanoen.2014.09.027

17. R. Zhao, Q. Li, C. Wang, L. Yin, Highly ordered mesoporous spinel $ZnCo_2O_4$ as a high-performance anode material for lithium-ion batteries. Electrochim. Acta **197**, 58–67 (2016). doi:10.1016/j.electacta.2016.03.047

18. D. Wang, X. Qi, H. Gao, J. Yu, Y. Zhao, G. Zhou, G. Li, Fabricating hierarchical porous $ZnCo_2O_4$ microspheres as high-performance anode material for lithium-ion batteries. Mater. Lett. **164**, 93–96 (2016). doi:10.1016/j.matlet.2015.10.126

19. Y. Sharma, N. Sharma, G.V. Subba, Rao, B.V.R. Chowdari, Nanophase $ZnCo_2O_4$ as a high performance anode material for Li-ion batteries. Adv. Funct. Mater. **17**(15), 2855–2861 (2007). doi:10.1002/adfm.200600997

20. Y. Deng, Q. Zhang, S. Tang, L. Zhang, S. Deng, Z. Shi, G. Chen, One-pot synthesis of $ZnFe_2O_4$/C hollow spheres as superior anode materials for lithium ion batteries. Chem. Commun. **47**(24), 6828–6830 (2011). doi:10.1039/c0cc05001f

21. J.F. Marco, J.R. Gancedo, M. Gracia, J.L. Gautier, E. Ríos, F.J. Berry, Characterization of the nickel cobaltite, $NiCo_2O_4$, prepared by several methods: an XRD, XANES, EXAFS, and XPS study. J. Solid State Chem. **153**(1), 74–81 (2000). doi:10.1006/jssc.2000.8749

22. V.M. Jiménez, A. Fernández, J.P. Espinós, A.R. González-Elipe, The state of the oxygen at the surface of polycrystalline cobalt oxide. J. Electron Spectrosc. Relat. Phenom. **71**(1), 61–71 (1995). doi:10.1016/0368-2048(94)02238-0

23. T. Choudhury, S.O. Saied, J.L. Sullivan, A.M. Abbot, Reduction of oxides of iron, cobalt, titanium and niobium by low-energy ion bombardment. J. Phys. D **22**(8), 1185 (1989). doi:10.1088/0022-3727/22/8/026

24. X.L. Wen, Z. Chen, Z. Liu, X. Lin, Structural and magnetic characterization of $ZnCo_2O_4$ thin film prepared by pulsed laser deposition. Appl. Surf. Sci. **357**(Part A), 1212–1216 (2015). doi:10.1016/j.apsusc.2015.09.152

25. A. Kumar, O.D. Jayakumar, V.M. Naik, G.A. Nazri, R. Naik, Improved electrochemical properties of solvothermally

synthesized Li_2FeSiO_4/C nanocomposites: a comparison between solvothermal and sol-gel methods. Solid State Ion **29**, 15–20 (2016). doi:10.1016/j.ssi.2016.06.014

26. X. Wang, Y. Liu, H. Arandiyan, H. Yang, L. Bai, J. Mujtaba, Q. Wang, S. Liu, H. Sun, Uniform Fe_3O_4 microflowers hierarchical structures assembled with porous nanoplates as superior anode materials for lithium-ion batteries. Appl. Surf. Sci. **389**, 240–246 (2016). doi:10.1016/j.apsusc.2016.07.105

27. Y. Zhang, J. Huang, Y. Ding, Porous Co_3O_4/CuO hollow polyhedral nanocages derived from metal-organic frameworks with heterojunctions as efficient photocatalytic water oxidation catalysts. Appl. Catal. B **198**, 447–456 (2016). doi:10.1016/j.apcatb.2016.05.078

28. S. Nilmoung, T. Sinprachim, I. Kotutha, P. Kidkhunthod, R. Yimnirun, S. Rujirawat, S. Maensiri, Electrospun carbon/$CuFe_2O_4$ composite nanofibers with improved electrochemical energy storage performance. J. Alloys Compd. **688**, 1131–1140 (2016). doi:10.1016/j.jallcom.2016.06.251

29. D. Narsimulu, B.N. Rao, M. Venkateswarlu, E.S. Srinadhu, N. Satyanarayana, Electrical and electrochemical studies of nanocrystalline mesoporous $MgFe_2O_4$ as anode material for lithium battery applications. Ceram. Int. **42**(15), 16789–16797 (2016). doi:10.1016/j.ceramint.2016.07.168

30. Y. Qin, M. Long, B. Tan, B. Zhou, RhB adsorption performance of magnetic adsorbent Fe_3O_4/RGO composite and its regeneration through a fenton-like reaction. Nano-Micro Lett. **6**(2), 125–135 (2014). doi:10.1007/BF03353776

31. Y. Pan, K. Ye, D. Cao, Y. Li, Y. Dong, T. Niu, W. Zeng, G. Wang, Nitrogen-doped graphene oxide/cupric oxide as an anode material for lithium ion batteries. RSC Adv. **4**(110), 64756–64762 (2014). doi:10.1039/C4RA13336F

32. C.T. Cherian, M. Zheng, M.V. Reddy, B.V. Chowdari, C.H. Sow, Zn_2SnO_4 nanowires versus nanoplates: electrochemical performance and morphological evolution during Li-cycling. ACS Appl. Mater. Inter. **5**(13), 6054–6060 (2013). doi:10.1021/am400802j

33. M.V. Reddy, G.V. Subba Rao, B.V.R. Chowdari, Nano-$(V_{1/2}Sb_{1/2}Sn)O_4$: a high capacity, high rate anode material for Li-ion batteries. J. Mater. Chem. **21**(27), 10003 (2011). doi:10.1039/c0jm04140h

34. C. Xiao, N. Du, H. Zhang, D. Yang, Improved cyclic stability of Mg_2Si by direct carbon coating as anode materials for lithium-ion batteries. J. Alloys Compd. **587**, 807–811 (2014). doi:10.1016/j.jallcom.2013.10.115

35. S. Xu, L. Lu, Q. Zhang, Q. Jiang, Z. Luo, S. Wang, G. Li, C. Feng, A facile synthesis of flower-like CuO as anode materials for lithium (sodium) ion battery applications. J. Nanosci. Nanotechnol. **16**(7), 7655–7661 (2016). doi:10.1166/jnn.2016.11593

36. H.W. Liu, H.F. Liu, Preparing micro/nano dumbbell-shaped CeO_2 for high performance electrode materials. J. Alloys Compd. **681**, 342–349 (2016). doi:10.1016/j.jallcom.2016.04.207

37. X.-B. Zhong, H.-Y. Wang, Z.-Z. Yang, B. Jin, Q.-C. Jiang, Facile synthesis of mesoporous $ZnCo_2O_4$ coated with polypyrrole as an anode material for lithium-ion batteries. J. Power Sources **296**, 298–304 (2015). doi:10.1016/j.jpowsour.2015.07.047

38. M. Nie, D. Chalasani, D.P. Abraham, Y. Chen, A. Bose, B.L. Lucht, Lithium ion battery graphite solid electrolyte interphase revealed by microscopy and spectroscopy. J. Phys. Chem. C **117**(3), 1257–1267 (2013). doi:10.1021/jp3118055

39. J. Li, J. Wang, D. Wexler, D. Shi, J. Liang, H. Liu, S. Xiong, Y. Qian, Simple synthesis of yolk-shelled $ZnCo_2O_4$ microspheres towards enhancing the electrochemical performance of lithium-ion batteries in conjunction with a sodium carboxymethyl cellulose binder. J. Mater. Chem. A **1**(48), 15292–15299 (2013). doi:10.1039/c3ta13787b

40. W. Luo, X. Hu, Y. Sun, Y. Huang, Electrospun porous $ZnCo_2O_4$ nanotubes as a high-performance anode material for lithium-ion batteries. J. Mater. Chem. **22**(18), 8916–8921 (2012). doi:10.1039/c2jm00094f